Figure S1

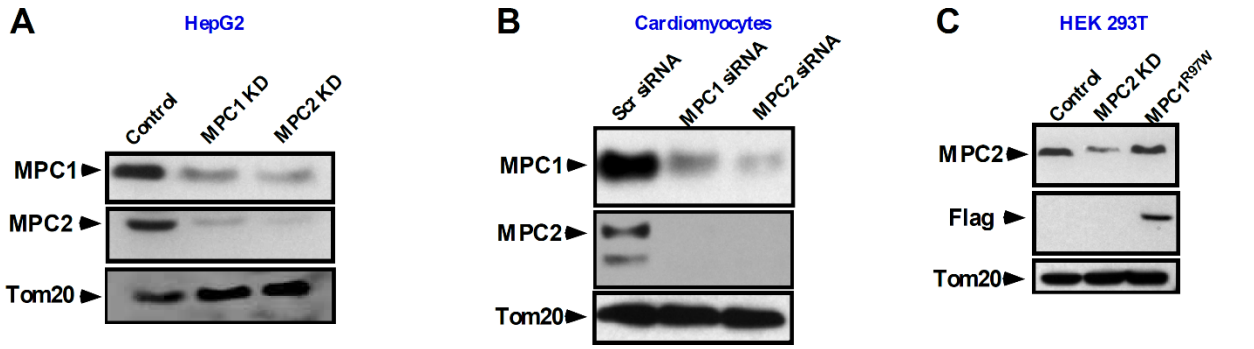

Figure S1: MPC1 and MPC2 abundance following RNAi-mediated knockdown.

A) MPC1 and MPC2 expression in HepG2 cells stably expressing either negative shRNA or lentiviral shRNA targeting different regions of *MPC1* and *MPC2* were assessed by Western blot analysis. TOM20 was used as a loading control. n = 3 independent experiments.

B) MPC1 and MPC2 expression in primary cardiomyocytes transfected with either scrambled siRNA or siRNA targeting different regions of *MPC1* and *MPC2*. 48 hours post transfection cells were collected and were assessed by Western blot analysis. TOM20 was used as a loading control. n = 3 independent experiments.

C) HEK293T cells stably expressing either negative shRNA or lentiviral shRNA targeting different regions of MPC2 and FLAG-tagged MPC1^{R97W} plasmid were assessed by Western blot analysis. TOM20 was used as a loading control. n = 3 independent experiments.

Figure S2

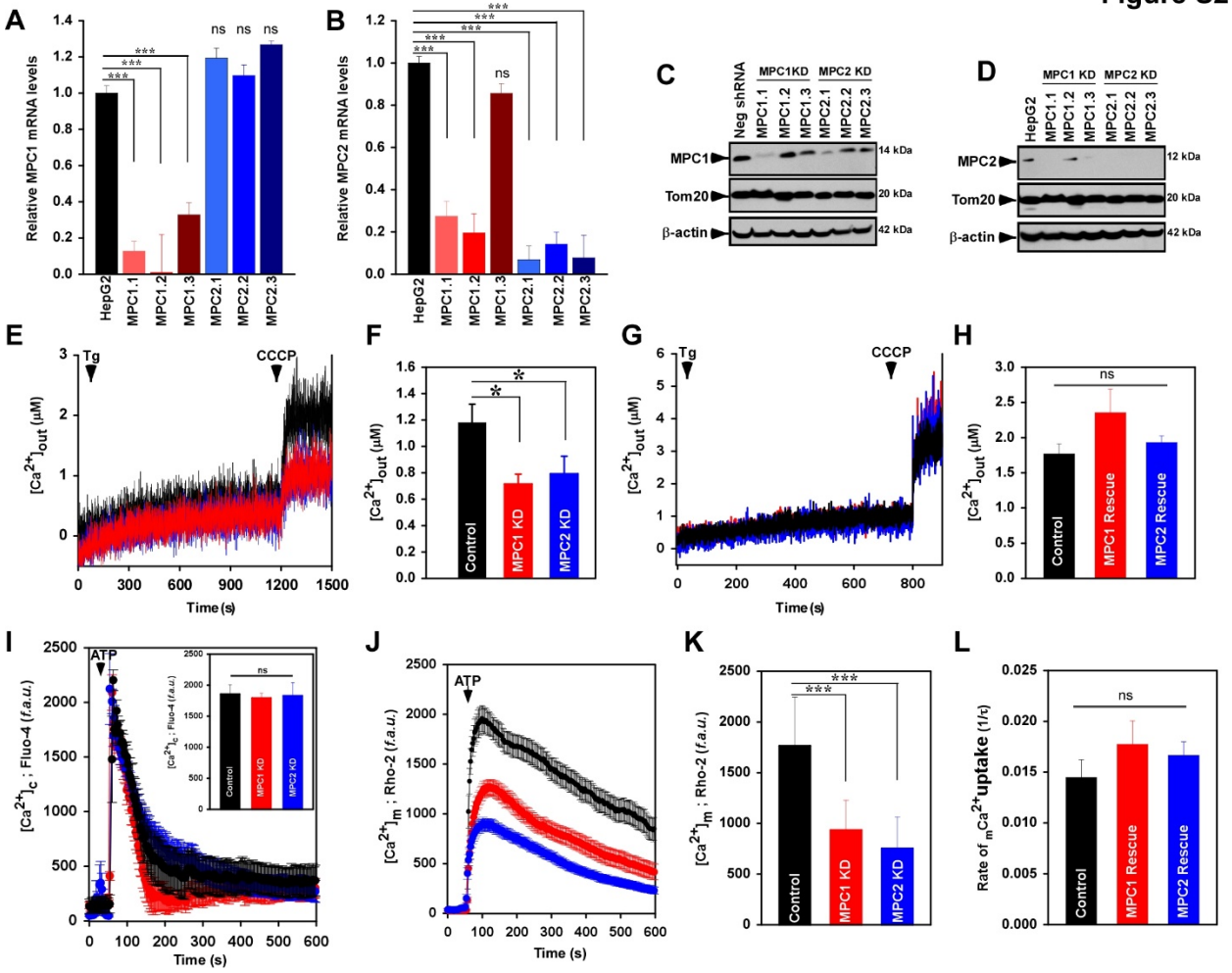

Figure S2: Silencing MPC alters mitochondrial Ca^{2+} uptake in a MICU1-dependent manner.

A and B) MPC1 and MPC2 expression in HepG2 cells stably expressing either negative shRNA or lentiviral shRNA targeting different regions of *MPC1* and *MPC2* were assessed by qRT-PCR. Data representative of 3-6 independent experiments.

C and D) MPC1 and MPC2 expression in HepG2 cells stably expressing either negative shRNA or lentiviral shRNA targeting different regions of *MPC1* and *MPC2* were assessed by Western blot analysis. Data representative of 3 independent experiments.

E) Representative traces of permeabilized (40 μg/ml digitonin) HepG2 control and MPC KD cells loaded with 2 μM thapsigargin (Tg) ratiometric Ca^{2+} indicator Fura2-FF and pulsed with 10 μM CCCP at 1200 s. MPC1 and MPC2 KD showed reduced matrix mitochondrial Ca^{2+}.

F) Quantitation of CCCP-induced Ca^{2+} release in control and MPC KD HepG2 cells from traces shown in (E). Data represent mean ± SEM (n=3 independent experiments), *P<0.05.

G) Representative traces of permeabilized (40 μg/ml digitonin) HepG2 control and MPC rescue cells loaded with 2 μM thapsigargin (Tg) ratiometric Ca^{2+} indicator Fura2-FF and pulsed with 10 μM CCCP at 1200 s.

H) Quantitation of CCCP-induced Ca^{2+} release in control and MPC rescue HepG2 cells from traces shown in (G). Data represent mean ± SEM (n=3 independent experiments), n.s., not significant.

I) Mean traces of $_{c}Ca^{2+}$ uptake as measured by Fluo-4 fluorescence in HepG2 WT, MPC1 and MPC2 KD cells upon stimulation with 10μM ATP. Inset: Quantified peak fluorescence. Data represent mean ± SEM (n=4 independent experiments), n.s., not significant

J) Mean traces of $_{m}Ca^{2+}$ uptake as measured by Rho-2 fluorescence in HepG2 WT, MPC1 KD and MPC2 KD cells upon stimulation with 10μM ATP.

K) Bar graph presents the peak fluorescence in HepG2 WT, MPC1 KD and MPC2 KD cells upon stimulation with 10μM ATP from traces shown in (J). Data represent mean ± SEM (n=3 independent experiments).

L) Bar graph presents the rate of $_{m}Ca^{2+}$ uptake in control and MPC rescue HepG2 cells. Data represent mean ± SEM (n=3 independent experiments). n.s., not significant.

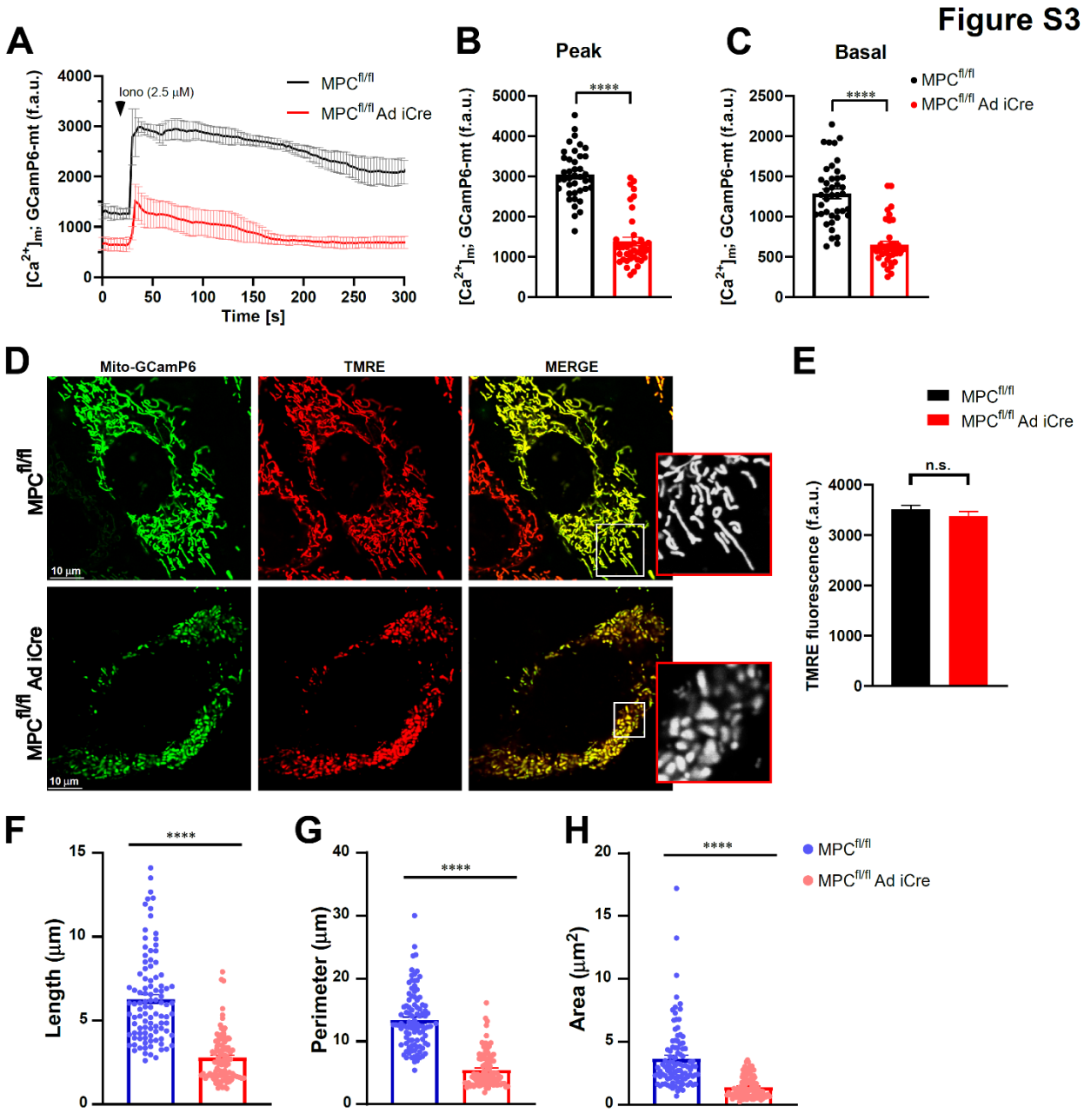

Figure S3. MPC1-deficient MEFs exhibit reduced MCU-mediated mitochondrial Ca^{2+} uptake and altered mitochondrial morphology.

A) Mean traces for $[Ca^{2+}]_m$ (GCaMP6-mt) fluorescence measured in *MPC1*$^{fl/fl}$ or *MPC1*$^{fl/fl}$ + Ad iCre MEFs. n = 4 independent experiments.

B) Quantification of peak mito-GCaMP6 fluorescence after ionomycin (2.5 μM) stimulation. Data represent mean ± SEM n=4 cells per group, 40 mitochondria per group. ****P<0.0001.

C) Quantification of basal mito-GCaMP6 fluorescence. Data represent mean ± SEM n=4 cells per group, 40 mitochondria per group. ****P<0.0001.

D) Assessment of MEFs mitochondrial morphology. MEFs were transduced with Ad-iCre virus, then with GCaMP6-mt 36 hours later, stained with TMRE 72 hours after transduction of Ad iCre virus, and imaged. Inset (gray scale) shows higher magnification images. n = 4 cells per group.

E) Quantification of TMRE fluorescence in *MPC1*$^{fl/fl}$ and *MPC1*$^{fl/fl}$ + Ad iCre hepatocytes. n = 4 cells per group, 15 mitochondria per cell. n.s., not significant.

F-H) Analyses of mitochondrial length, area, and perimeter. Mean ± SEM. n = 4 cells per group, 20 mitochondria per cell. ****P<0.0001.

Figure S4

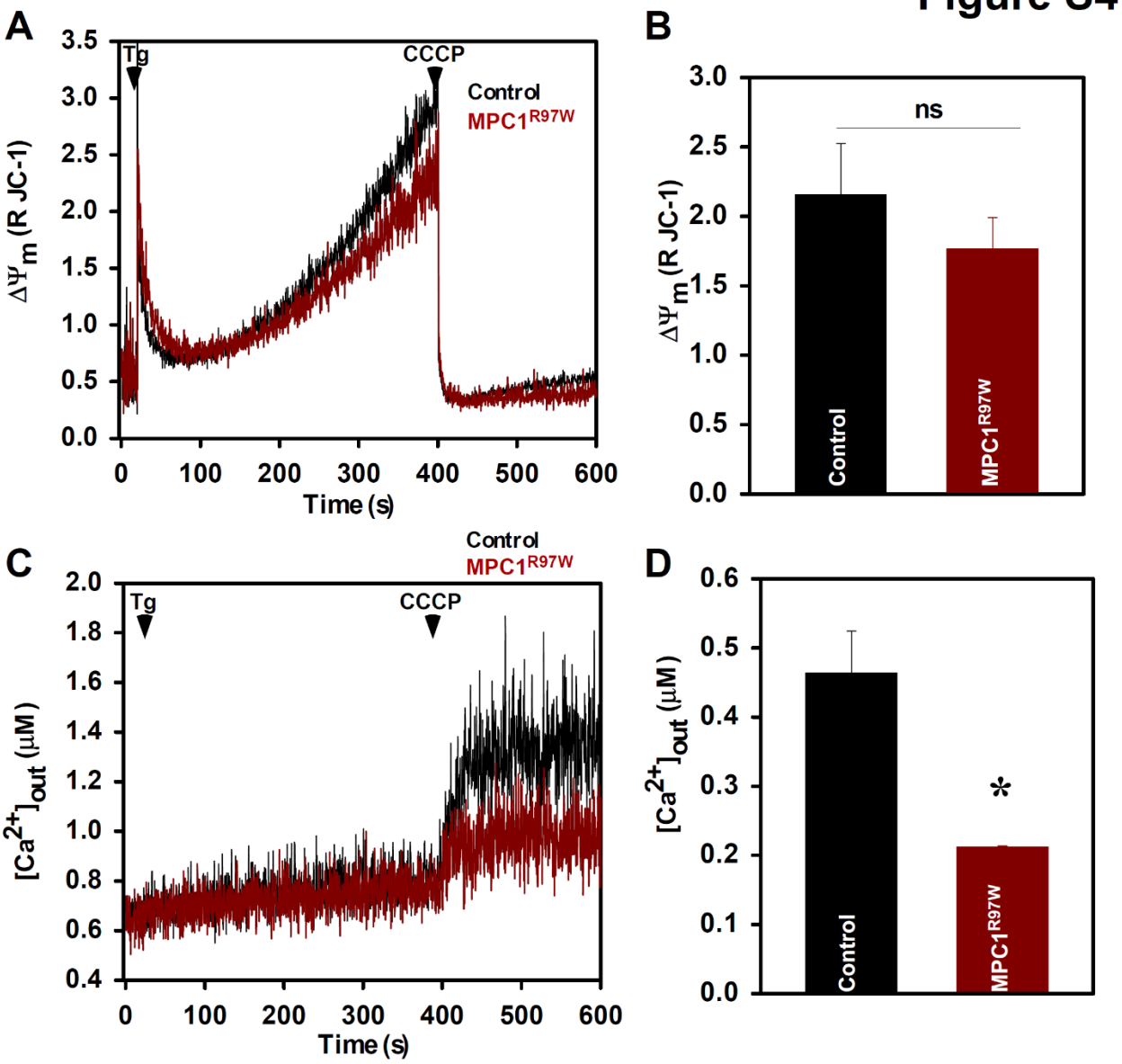

Figure S4: Pyruvate carrier mutations result in decreased matrix Ca^{2+} in a MICU1-dependent manner.

A) Representative traces of permeabilized (40 μg/ml digitonin) HepG2 control and $MPC1^{R97W}$ cells loaded with 2 μM thapsigargin (Tg), ratiometric $\Delta\Psi_m$ fluorophore JC-1 and pulsed with 10 μM uncoupler CCCP at 400 s.

B) Quantitation of $\Delta\Psi_m$ before addition of CCCP in control and MPC1^{R97W} HepG2 cells from traces in (A). Data represent mean ± SEM (n=3 independent experiments), n.s., not significant

C) Representative traces of permeabilized (40 µg/ml digitonin) HepG2 control and MPC1^{R97W} cells loaded with 2 µM thapsigargin (Tg) ratiometric Ca^{2+} indicator Fura2-FF and pulsed with 10 µM uncoupler CCCP at 400 s.

D) Quantitation of CCCP-induced Ca^{2+} release in control and MPC1^{R97W} HepG2 cells from traces in (C). Data represent mean ± SEM (n=3 independent experiments), *P<0.05.

Figure S5

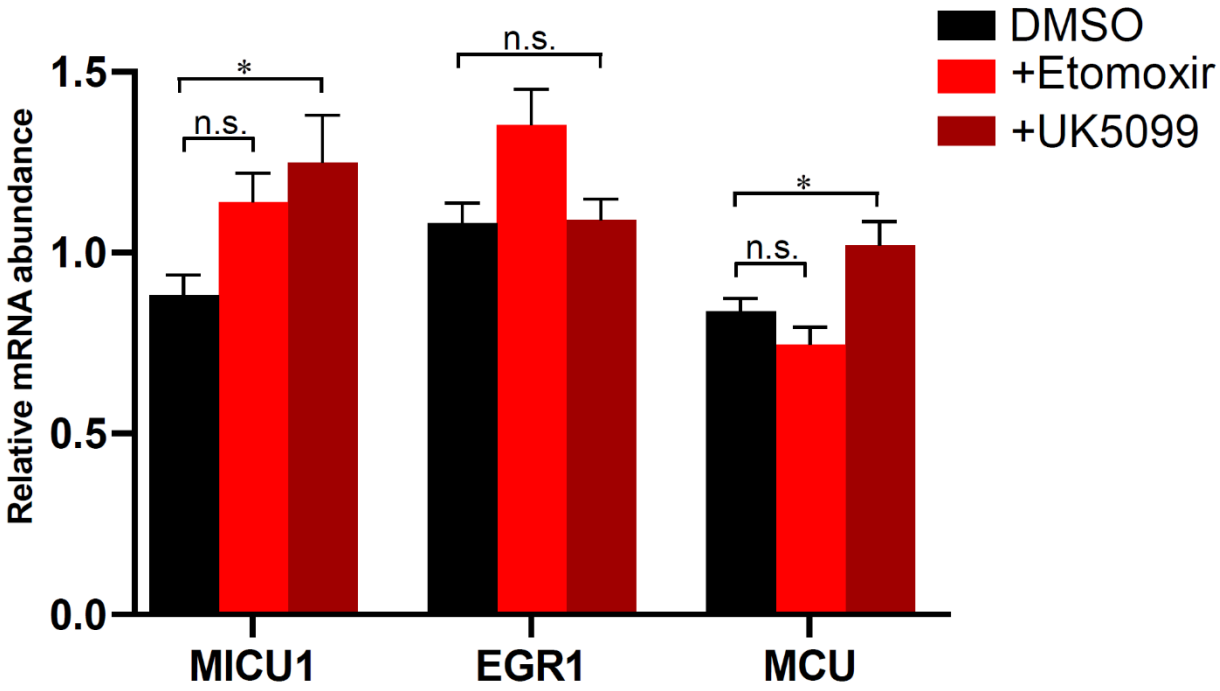

Figure S5: Pharmacologic blockade of fatty acid and pyruvate flux by etomoxir and UK5099 enhances *MICU1* mRNA abundance.

WT murine hepatocytes were treated with etomoxir (10 μM) or UK5099 (100 μM) for 24 hours. Total mRNA was isolated, and RT-qPCR was performed to measure *MICU1*, *EGR1*, and *MCU* mRNA abundance. The relative changes were normalized using β-actin. Data represent mean ± SEM from n=3 independent experiments, *P<0.05, n.s. not significant.